Pergamon

Int. J. Heat Mass Transfer. Vol. 39, No. 4, pp. 745–752, 1996

0017-9310/96 $15.00 + 0.00

0017-9310(95)00163-8

Laminar mixed convection in vertical elliptic ducts

K. VELUSAMY
Thermal Hydraulics Section, Indira Gandhi Centre for Atomic Research, Kalpakkam 603102, India

and

VIJAY K. GARG†
AYT Corporation, c/o NASA Lewis Research Center, Mail Stop 5-11, Cleveland, OH 44135, U.S.A.

(*Received* 7 *November* 1994 *and in final form* 20 *April* 1995)

Abstract—A control volume based numerical solution is described for the fully developed mixed convection in vertical ducts of elliptic cross-section. The duct wall is supplied with a uniform axial heat rate while the thickness and thermal conductivity of the duct wall are such that the wall temperature is circumferentially uniform. Results for velocity and temperature distributions, friction factor, Nusselt number and critical Rayleigh number are presented for a wide range of duct aspect ratios and Rayleigh numbers. It is found that during mixed convection, fluid with a higher axial velocity exists around the foci of the elliptical cross-section, leading to substantial heat transfer enhancement in this region of the duct. The ratio of friction factor during mixed convection to that during forced convection is low in elliptical ducts compared to that in a circular duct. Also, the ratio of Nusselt number to friction factor is higher for elliptic ducts compared to that for a circular duct, irrespective of the value of the Rayleigh number. The critical Rayleigh number, at which flow reversal is initiated in the core region, is higher for elliptic ducts compared to that for a circular duct.

1. INTRODUCTION

In many heat transfer applications temperature rise of the fluid participating in energy transfer is high enough for the effect of buoyancy to be significant. This free convection effect distorts the velocity and temperature distribution of the fluid in ducts considerably, leading to higher values of friction factor and heat transfer coefficient than those in the forced convection regime alone (cf. Prakash and Patankar [1]). In modern engineering equipment, non-circular ducts are being used in increasing numbers as is evident from the growing literature in this field (cf. Shah and London [2], and Kakac *et al.* [3]).

Fully developed mixed convection in vertical ducts has been investigated by numerous authors. Of them, Morton [4] and Tao [5] presented analytical solutions for flow through circular ducts, while Prakash and Patankar [1] presented numerical results for internally finned circular ducts. Maitra and Subba Raju [6] analyzed flow through concentric cylindrical annuli, while Sathyamurthy *et al.* [7] analyzed flow through eccentric cylindrical annuli. Han [8] analyzed the case of rectangular ducts with heat generation in the fluid, while Tao [9] analyzed rectangular as well as parallel plate ducts with and without heat generation. Flow through circular ducts was studied by Lu [10], while flow through triangular ducts with heat generation was analyzed by Aggarwala and Iqbal [11] employing membrane analogy. Later Iqbal *et al.* [12] employed a variational formulation to analyze flow through triangular and rhombic ducts. References [1, 4–12] deal with circumferentially uniform wall temperature and uniform axial heat rate.

Iqbal *et al.* [13] presented a point matching solution for flow through polygonal ducts for the conditions of uniform circumferential heat flux as well as uniform circumferential temperature on the duct walls. Later Iqbal *et al.* [14] presented a variational solution for arbitrary shaped ducts including elliptic ducts. However, they considered circumferentially uniform wall heat flux only, and did not investigate the critical Rayleigh number at which flow reversal takes place; the range of Rayleigh numbers considered by them is 0–5000 only. The condition of circumferentially uniform wall temperature is more important especially in cases where the duct wall is thick and is made up of highly conducting material. A review of heat transfer literature dealing with flow through elliptical ducts [3, 15–26] indicates that the solution for fully developed mixed convection in vertical elliptic ducts with circumferentially uniform wall temperature and uniform axial heat rate has not been reported. The present analysis aims to fill this gap.

2. ANALYSIS

We consider steady, fully developed, laminar flow of a Newtonian fluid in a vertical elliptic duct, and

† Author to whom correspondence should be addressed.

NOMENCLATURE

a, b semi major and minor axes of the elliptical section, respectively
c focal distance of the elliptical section
C_p specific heat of the fluid
D hydraulic diameter of the elliptical section, $\pi b/E(m)$
$E(m)$ complete elliptic integral of second kind
f_0 friction factor during forced convection
f friction factor during mixed convection
g acceleration due to gravity
$\bar{h}$ circumferentially averaged heat transfer coefficient
H $(c/D)(\sinh^2\eta+\sin^2\xi)^{1/2}$
k thermal conductivity of the fluid
m $(1-\lambda^2)^{1/2}$
Nu average Nusselt number during mixed convection
Nu_0 average Nusselt number during forced convection
n_ψ number of control volumes in the cross-section for the variable ψ
p dimensional pressure
p^* non-gravitational pressure, $p+\rho_0 gz$
P dimensionless pressure, $p^*D/(\mu\bar{w}Re)$
$\dot{Q}'$ heat rate per unit duct length, $\pi ab\rho_0\bar{w}Cp\ \mathrm{d}t_m/\mathrm{d}z$
$r_{i\psi}$ residue of the discretized equation for ith control volume for the variable ψ
Ra Rayleigh number, $\beta g(\mathrm{d}t_m/\mathrm{d}z)D^4/(\nu\alpha)$
Ra_c critical Rayleigh number = one at which reverse flow is initiated
Re Reynolds number, $\bar{w}D/\nu$
R_ψ absolute sum of $r_{i\psi}$ taken over n_ψ
t temperature of the fluid
t_m mean temperature of the fluid
t_w temperature of the duct wall
T dimensionless temperature, $k(t-t_w)/\dot{Q}'$
T_m dimensionless mean temperature
w axial velocity in the duct
$\bar{w}$ average axial velocity in the duct
W dimensionless counterpart of w, $w/\bar{w}$
W_{max} maximum value of W
x cross-stream Cartesian coordinate (Fig. 1)
y cross-stream Cartesian coordinate (Fig. 1)
z axial coordinate (along the flow direction)
Z dimensionless axial coordinate, $z/(DRe)$.

Greek symbols

α thermal diffusivity of the fluid
β coefficient of volumetric expansion
ε a small number for checking convergence
η elliptic cylinder coordinate (Fig. 1)
η_w value of η at the curved wall
λ aspect ratio of the duct, b/a
μ dynamic viscosity of the fluid
ν kinematic viscosity of the fluid
ρ_0 density of the fluid at $t = t_w$
Φ dimensionless temperature of fluid, T/T_m
Φ_{max} maximum value of ϕ
ξ elliptic cylinder coordinate (Fig. 1).

analyze the case where buoyancy aids the flow, that is, if the flow is upwards the fluid is being heated (heated upflow), and if the flow is downwards the fluid is being cooled (cooled downflow). The other situations of heated downflow and cooled upflow are not of much practical significance [1] and are therefore not considered. A uniform heat rate per unit duct length is imposed on the duct. The duct wall is thick and made up of highly conducting material so that at any axial location the wall temperature is circumferentially uniform. At moderate velocities, viscous dissipation and compression work are considered negligible. The fluid properties are also considered constant except for density for which the well known Boussinesq approximation is used.

We use elliptic cylinder coordinates (ξ, η, z) as shown in Fig. 1. This coordinate system consists of an orthogonal family of confocal ellipses and hyperbolas in a plane, translated in the third (axial here) direction normal to the plane. The surfaces η = constant are the confocal elliptic cylinders

$$\frac{x^2}{(c\cosh\eta)^2}+\frac{y^2}{(c\sinh\eta)^2}=1$$

while the surfaces ξ = constant are the hyperbolic cylinders

$$\frac{x^2}{(c\cos\xi)^2}-\frac{y^2}{(c\sin\xi)^2}=1.$$

The normalized equations for conservation of momentum, mass and energy are

Axial momentum:

$$\frac{1}{H^2}\left[\frac{\partial^2 W}{\partial\xi^2}+\frac{\partial^2 W}{\partial\eta^2}\right]=\frac{\mathrm{d}P}{\mathrm{d}Z}-\frac{[E(m)]^2}{\pi\lambda}RaT \quad (1)$$

Integral continuity:

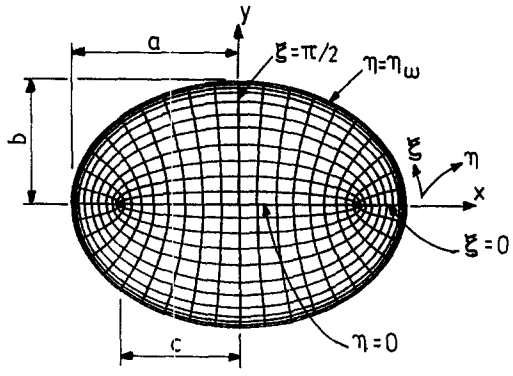

Fig. 1. Elliptic-cylinder coordinate system.

$$\int_{\xi=0}^{\pi/2}\int_{\eta=0}^{\eta_w} WH^2\,\mathrm{d}\xi\,\mathrm{d}\eta = \frac{[E(m)]^2}{4\pi\lambda} \tag{2}$$

Energy equation:

$$\frac{1}{H^2}\left[\frac{\partial^2 T}{\partial\xi^2}+\frac{\partial^2 T}{\partial\eta^2}\right]=\frac{\pi\lambda W}{[E(m)]^2} \tag{3}$$

where the variables are defined in the Nomenclature. Owing to symmetry, only a quarter of the duct needs to be considered for analysis. Equations (1) and (3) are therefore subject to the following boundary conditions:

$$\begin{aligned} &W=0=T && \text{along } \eta=\eta_w && \text{for all } \xi\\ &\partial W/\partial\xi=0=\partial T/\partial\xi && \text{along } \xi=0,\pi/2 && \text{for all } \eta\\ &\partial W/\partial\eta=0=\partial T/\partial\eta && \text{along } \eta=0 && \text{for all } \xi. \end{aligned} \tag{4}$$

From first principles and definitions given in the Nomenclature, the product of friction factor and Reynolds number is given by

$$fRe = (1/2)\,\mathrm{d}P/\mathrm{d}Z$$

and the Nusselt number is

$$Nu=\frac{\bar{h}D}{k}=-\frac{1}{4T_m}\frac{\pi\lambda}{[E(m)]^2} \tag{5}$$

where

$$T_m=\frac{4\pi\lambda}{[E(m)]^2}\int_{\xi=0}^{\pi/2}\int_{\eta=0}^{\eta_w} WTH^2\,\mathrm{d}\xi\,\mathrm{d}\eta. \tag{6}$$

In equations (1)–(3) the governing parameters are the Rayleigh number, Ra, and the duct aspect ratio, λ.

3. SOLUTION

Numerical solution to the set of coupled governing equations (1)–(4) is obtained iteratively by employing the control volume based discretization method [27]. The axial pressure gradient in the duct is evaluated via the integral continuity equation using the method proposed by Raithby and Schneider [28]. The discretization procedure yields a set of algebraic equations for each variable. The pentadiagonal system of algebraic equations for each variable is solved by a plane-by-plane method [29]. This method is an extension of the Thomas algorithm for the tridiagonal system of equations. Convergence is assumed once the absolute sum of the residue R_ψ corresponding to the variable ψ in the discretization equation is less than ε where

$$R_\psi=\sum_{i=1}^{n_\psi}|r_{i\psi}|.$$

The value of ε is taken to be 10^{-5} for the results presented here. Solutions for higher values of Rayleigh number are obtained starting with lower Rayleigh number solutions as the initial guess. This reduces the number of iterations for convergence. Relaxation factors in the range 0.1–0.5 are used. The relaxation factor is lower for higher values of Rayleigh number and lower values of the aspect ratio.

All results presented here for elliptic ducts were obtained on two grid patterns in the cross-stream (ξ–η) plane, namely a 22×22 and a 42×42 grid. The coarse grid size is exactly double the fine grid size. Grids were packed near the duct wall where large velocity and temperature gradients exist. For $\lambda=0.1$, Table 1 compares the friction factor, Nusselt number and the maximum velocity in the duct for the two grid patterns at various Rayleigh numbers. The maximum difference occurs at the highest Rayleigh number but is only 1.2% in the maximum velocity, and less than 0.1% in friction factor and Nusselt number. Similar results were obtained for other aspect ratios as well. Hence the grid pattern of 42×42 is satisfactory.

Table 1. Comparison of coarse and fine grid results for $\lambda=0.1$

	W_{max}		$2fRe$		Nu	
Ra	Grid 22×22	Grid 42×42	Grid 22×22	Grid 42×42	Grid 22×22	Grid 42×42
0	1.994	1.999	38.57	38.61	5.124	5.125
6000	1.920	1.922	251.98	252.13	8.259	8.252
20 000	2.514	2.520	614.29	615.00	10.894	10.879
38 000	2.869	2.904	991.25	992.13	12.889	12.878

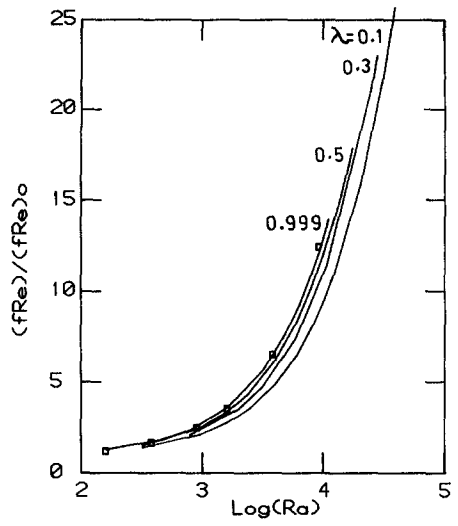

Fig. 2. Effect of Rayleigh number on friction factor; □, numerical solution for circular tubes by Prakash and Patankar [1].

4. ACCURACY

In order to verify the computer program, the well studied problem of mixed convection through a vertical circular duct was computed first. The aspect ratio for this study was taken to be 0.999 since the coordinate transformation is singular for $\lambda = 1$. The predicted variation of friction factor and Nusselt number with Rayleigh number is shown in Figs. 2 and 3. Also shown in these figures are the numerical results of Prakash and Patankar [1]. Clearly, the comparison is excellent. The case of pure forced convection in elliptic ducts was also computed. The present results for friction factor and Nusselt number are compared with the results reported by Shah and London [2] in Table 2. The comparison is again very good.

Table 2. Results for pure forced convection; comparison with ref. [2], p. 248

	fRe		*Nu*	
λ	Present	Ref. [2]	Present	Ref. [2]
0.7	16.238	16.244	4.417	4.422
0.5	16.819	16.823	4.552	4.558
0.3	17.889	17.896	4.802	4.803
0.1	19.307	19.314	5.125	5.124

5. RESULTS AND DISCUSSION

Results were obtained for aspect ratio λ varying from 0.1 to 0.999. Since fully developed flows involving reverse flows are unlikely in a practical situation, the Rayleigh number was varied from zero to a value at which flow reversal takes place. This critical value of the Rayleigh number depends upon the aspect ratio.

The ratios (f/f_0 and Nu/Nu_0) of friction factor and Nusselt number during mixed convection to those in pure forced convection are shown in Figs. 2 and 3 as a function of *Ra* for various λ. It is clear from Fig. 2 that f/f_0 increases with *Ra* for elliptic ducts, much like that for a circular duct. For a given Rayleigh number, the value of f/f_0 increases with the aspect ratio. From Fig. 3, it is clear that Nu/Nu_0 also increases with *Ra*, similar to f/f_0, but at a much slower rate. Up to $Ra = 3800$, the value of Nu/Nu_0 is high for low aspect ratios. However, for $Ra > 3800$, the contrary is true. In order to compare elliptic ducts with circular ones, the value of *Nu/fRe* is plotted in Fig. 4. It is seen that when the aspect ratio is lower, the ratio *Nu/fRe* is

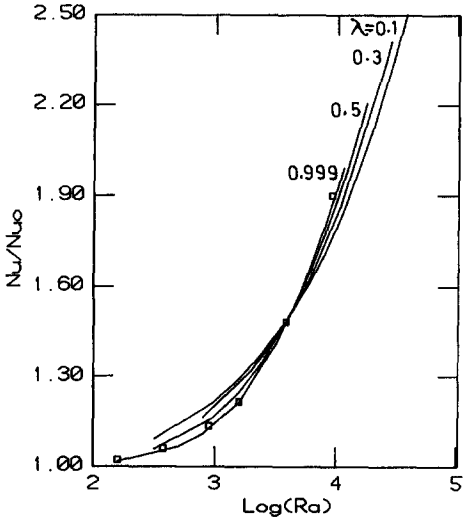

Fig. 3. Effect of Rayleigh number on Nusselt number; □, numerical solution for circular tubes by Prakash and Patankar [1].

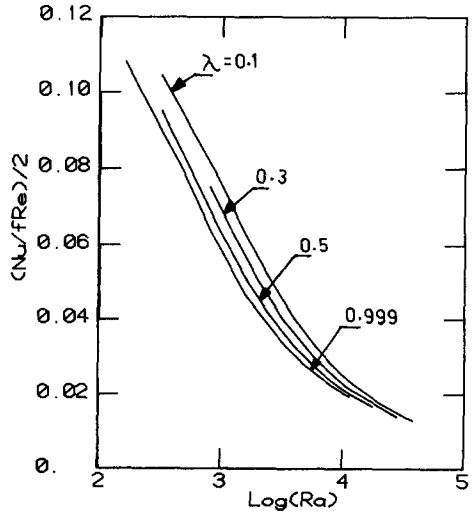

Fig. 4. Effect of Rayleigh number on the ratio (*Nu/fRe*).

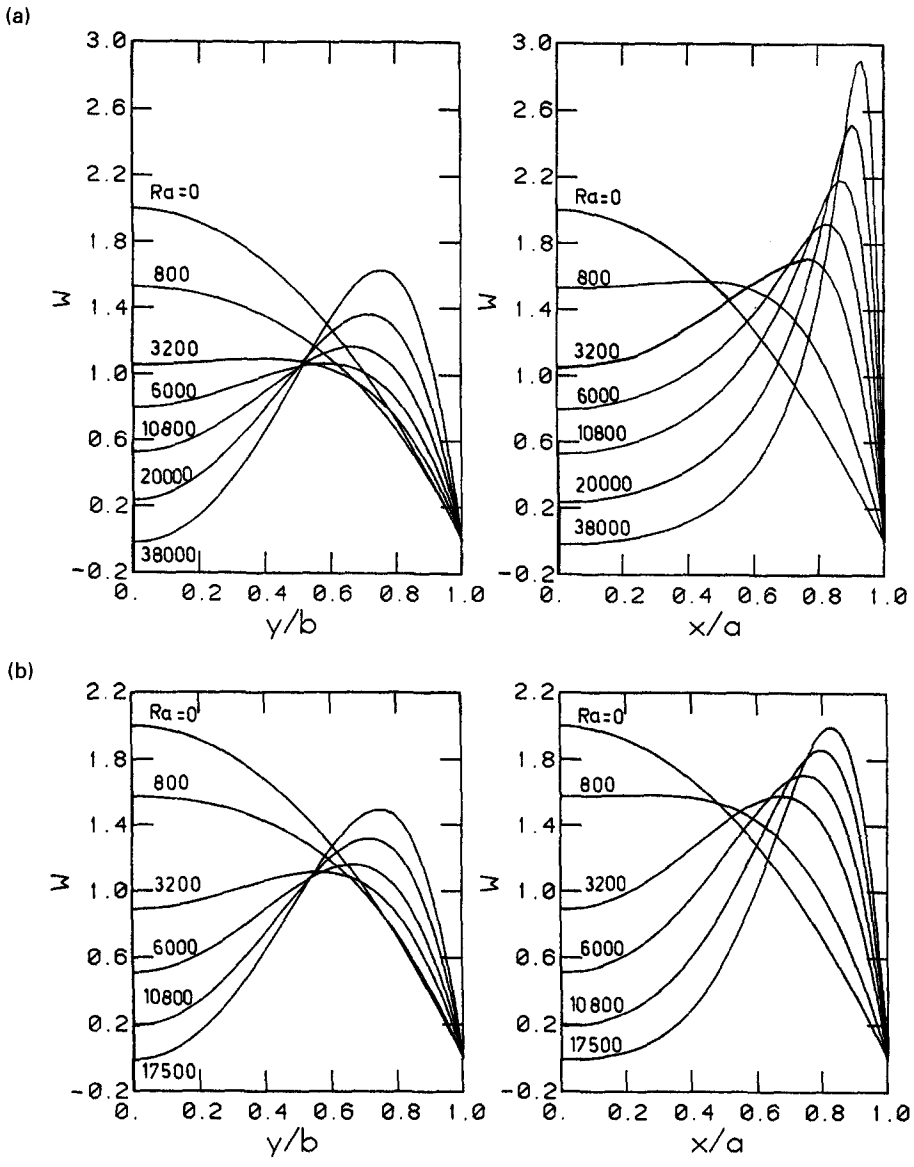

Fig. 5. Dimensionless axial velocity along the minor and major axes; (a) ($\lambda = 0.1$); (b) ($\lambda = 0.5$).

higher for the entire range of Rayleigh numbers analyzed. However, the superiority of elliptic ducts over circular ones is not significant for very high values of the Rayleigh number.

The distribution of axial velocity along the minor and major axes of the duct are presented in Figs. 5(a) and (b) for aspect ratios 0.1 and 0.5, respectively. It can be seen that as *Ra* increases, the fluid adjacent to the duct wall is accelerated and that in the core is decelerated. This holds for all values of the aspect ratio. Also, the velocity values on the major axis are higher than those on the minor axis for all values of λ and *Ra*. For a given *Ra*, the lower the value of λ, the lower is the maximum velocity along the minor axis, and higher is the maximum velocity along the major axis. This implies that as ellipticity increases, the flow is distributed with increased non-uniformity at a given value of *Ra*. Also, the location of maximum velocity along the major axis moves towards the wall as λ decreases at a given Rayleigh number.

The temperature distribution along the minor and major axes of the duct are shown in Figs. 6(a) and (b) for aspect ratios 0.1 and 0.5, respectively. It is obvious from these figures that the temperature distribution is more uniform for higher values of *Ra*. Also, for elliptic ducts, the heat flux is quite non-uniform along the duct circumference, unlike that in a circular duct. The heat flux is higher in the flatter region of the duct compared to that in the curved region. This is evident from the fact that for $\lambda = 0.1$, the ratio of heat flux

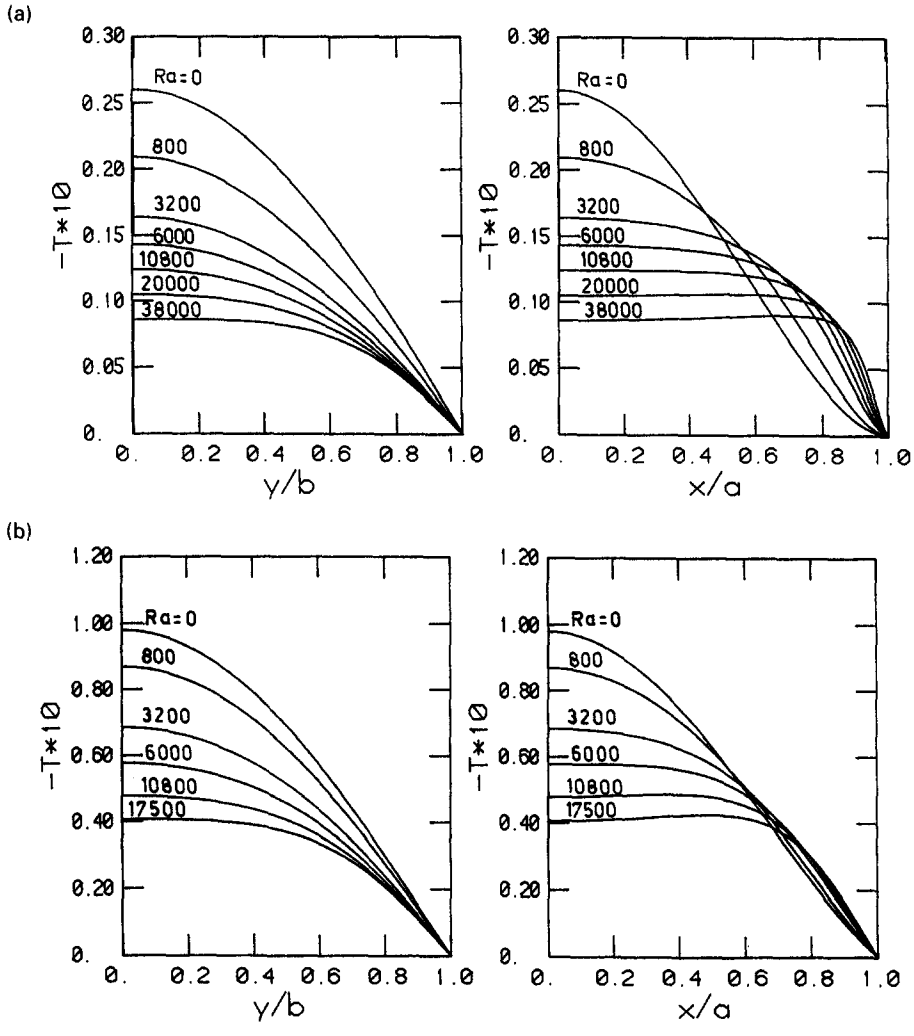

Fig. 6. Dimensionless temperature along the minor and major axes; (a) ($\lambda = 0.1$); (b) ($\lambda = 0.5$).

along the minor axis to that along the major axis is about three for the highest *Ra* of 38 000. For a given axial heat rate, heat flux in the curved region increases dramatically with *Ra*. This is more so for lower values of λ. A reason for this behavior is the existence of higher axial velocity fluid around the foci of the duct. Comparing Fig. 6(a) with 6(b), it is clear that uniformity in temperature increases with ellipticity for a given Rayleigh number.

Shown in Figs. 7(a)–(c) are the contours of dimensionless axial velocity (right half) and temperature (left half) for various values of λ and *Ra*. The contours are shown at intervals of 0.1. The locations of maximum axial velocity and temperature are also indicated with an $\times$. It can be observed from these figures that as buoyancy increases, higher axial velocities exist around the foci of the elliptic duct. The concentration of iso-W curves near the foci and increase of W_{max} leads to increased wall shear at higher values of *Ra*. For low values of *Ra* and high values of λ, the temperature contours are nearly concentric ellipses. However, the contours get considerably distorted for high values of *Ra* and low values of λ. The location of maximum temperature shifts away from the duct center as *Ra* increases. With increasing *Ra*, the higher concentration of isotherms near the foci indicates enhanced heat flux in that region of the duct. This is the outcome of larger momentum of the fluid in that region.

As pointed out already, the acceleration of fluid adjacent to the duct wall leads to retardation in the core region. At a certain value of Rayleigh number, known as the flow-reversal or critical Rayleigh number, the core-region flow gets reversed. The critical Rayleigh number is plotted against the duct aspect ratio in Fig. 8. For mildly elliptic ducts ($\lambda \leqslant 0.7$), the critical Rayleigh number is close to the circular duct value of nearly 10^4. However, as the aspect ratio falls

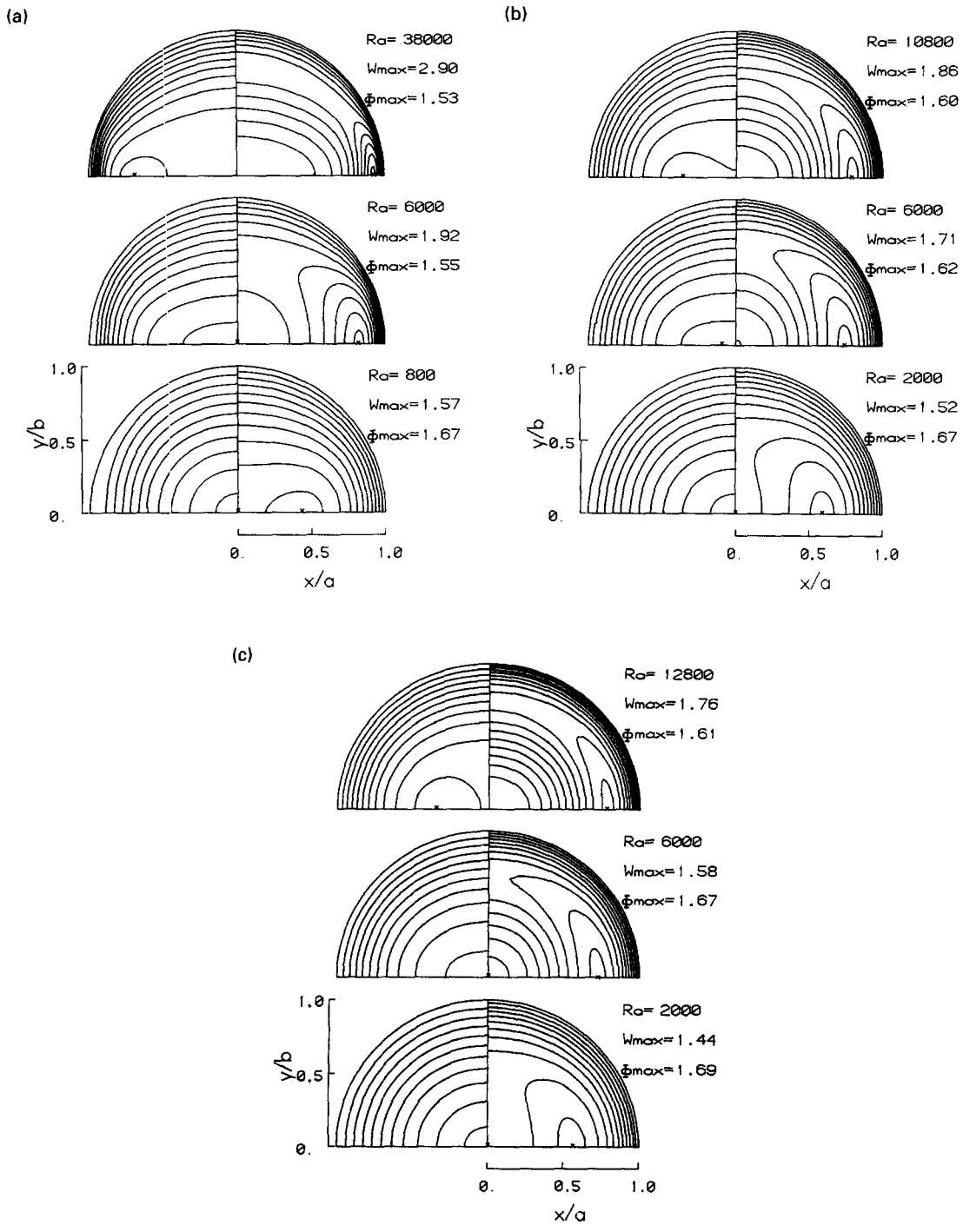

Fig. 7. Isotherms and iso-axial velocity contours; (a) ($\lambda = 0.1$); (b) ($\lambda = 0.5$); (c) ($\lambda = 0.7$).

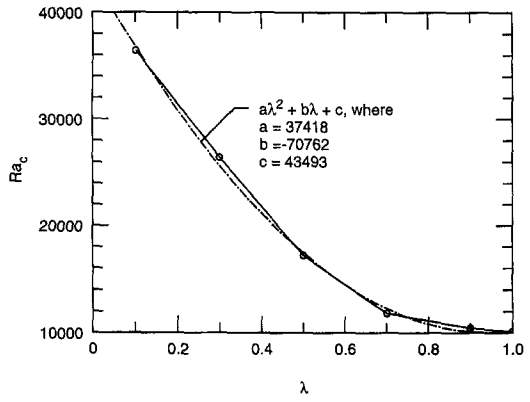

Fig. 8. Critical Rayleigh number vs the aspect ratio.

below 0.5, the critical *Ra* increases sharply. This implies that a stronger buoyancy is required to reverse the flow in elliptic ducts than that in circular ducts.

6. CONCLUSIONS

The problem of fully developed, laminar mixed convection in vertical elliptic ducts with uniform axial heat rate and circumferentially uniform wall temperature has been analyzed. Numerical results based on a control volume based discretization method have been presented for a wide range of parameters. The following are the main conclusions.

(1) During mixed convection in elliptical ducts, fluid with a high axial velocity exists around the foci.

(2) For a given Rayleigh number, the lower the aspect ratio, the higher is the maximum velocity and the closer it is to the foci of the duct.

(3) For the entire range of Rayleigh numbers, the ratio of Nusselt number to the friction factor is high when the aspect ratio is low.

(4) The critical Rayleigh number is higher for lower values of the aspect ratio.

Acknowledgements—The first author would like to thank S. B. Bhoje, S. C. Chetal and G. Vaidyanathan of Reactor Group, IGCAR, for their encouragement and support, and P. Sreenivasan of the IGCAR Computer Centre for the use of computing facilities.

REFERENCES

1. C. Prakash and S. V. Patankar, Combined free and forced convection in vertical tubes with radial internal fins, *J. Heat Transfer* **103,** 566–572 (1981).
2. R. K. Shah and A. L. London, *Laminar Flow Forced Convection in Ducts*. Academic Press, New York (1978).
3. S. Kakac, R. K. Shah and W. Aung, *Handbook of Single Phase Convection Heat Transfer*. Wiley Interscience, New York (1987).
4. B. R. Morton, Laminar convection in uniformly heated pipes, *J. Fluid Mech.* **12,** 227–240 (1959).
5. L. N. Tao, Heat transfer of combined free and forced convection in circular and sector tubes, *Appl. Sci. Res.* **9A,** 357–368 (1960).
6. D. Maitra and K. Subba Raju, Combined free and forced convection laminar heat transfer in a vertical annulus, *J. Heat Transfer* **97,** 135–137 (1975).
7. P. Sathyamurthy, K. C. Karki and S. V. Patankar, Laminar fully developed mixed convection in a vertical eccentric annulus, *Numer. Heat Transfer* **22A,** 71–85 (1992).
8. L. S. Han, Laminar heat transfer in rectangular channels, *J. Heat Transfer* **81,** 121–128 (1959).
9. L. N. Tao, On combined free and forced convection in channels, *J. Heat Transfer* **82,** 233–238 (1960).
10. P. C. Lu, Combined free and forced convection heat generating laminar flow inside vertical pipes with circular sector cross section, *J. Heat Transfer* **82,** 227–232 (1960).
11. B. D. Aggarwala and M. Iqbal, On limiting Nusselt numbers from membrane analogy for combined free and forced convection through vertical ducts, *Int. J. Heat Mass Transfer* **12,** 737–748 (1969).
12. M. Iqbal, B. D. Aggarwala and A. C. Fowler, Laminar combined free and forced convection in vertical noncircular ducts under uniform heat flux, *Int. J. Heat Mass Transfer* **12,** 1123–1139 (1969).
13. M. Iqbal, S. A. Ansari and B. D. Aggarwala, Effect of buoyancy on forced convection in vertical regular polygonal ducts, *J. Heat Transfer* **92,** 237–244 (1970).
14. M. Iqbal, A. K. Khatry and B. D. Aggarwala, On the second fundamental problem of combined free and forced convection through vertical noncircular ducts, *Appl. Sci. Res.* **26,** 183–208 (1972).
15. D. E. Gilbert, R. W. Leay and H. Barrow, Theoretical analysis of forced laminar convection heat transfer in the entrance region of an elliptic duct, *Int. J. Heat Mass Transfer* **16,** 1501–1503 (1973).
16. C. Chiranjivi and A. Ravi Prasad, Study of laminar flow friction in elliptical conduits, *Ind. J. Technol.* **12,** 87–90 (1974).
17. S. S. Rao, D. C. Raju and M. V. Ramana Rao, Pressure drop studies in elliptic ducts, *Ind. J. Technol.* **13,** 6–11 (1975).
18. M. A. Ebadian, H. C. Topakoglu and O. A. Arnas, On the convective heat transfer in a tube of elliptic cross-section maintained under constant wall temperature, *J. Heat Transfer* **108,** 33–39 (1986).
19. M. S. Bhatti, Heat transfer in the fully developed region of elliptical ducts with uniform wall heat flux, *J. Heat Transfer* **106,** 895–898 (1984).
20. M. S. Bhatti, Laminar flow in the entrance region of elliptical ducts, *J. Fluids Engng* **105,** 290–296 (1983).
21. V. K. Garg and K. Velusamy, Developing flow in an elliptical duct, *Int. J. Engng Fluid Mech.* **2**(2), 177–196 (1989).
22. R. M. Abdel-Wahed, A. E. Attia and M. A. Hifni, Experiments on laminar flow and heat transfer in an elliptical duct, *Int. J. Heat Mass Transfer* **27,** 2397–2413 (1984).
23. Z. F. Dong and M. A. Ebadian, A numerical analysis of thermally developing flow in elliptic ducts with internal fins, *Int. J. Heat Fluid Flow* **12,** 166–172 (1991).
24. Z. F. Dong and M. A. Ebadian, Numerical analysis of laminar flow in curved elliptic ducts, *J. Fluids Engng* **113,** 555–562 (1991).
25. Z. F. Dong and M. A. Ebadian, Effects of buoyancy on laminar flow in curved elliptic ducts, *J. Heat Transfer* **114,** 936–943 (1992).
26. Z. F. Dong and M. A. Ebadian, Convective and radiative heat transfer in the entrance region of an elliptic duct with fins, *Numer. Heat Transfer* **21A,** 91–107 (1992).
27. S. V. Patankar, *Numerical Heat Transfer and Fluid Flow*. McGraw-Hill, New York (1980).
28. G. D. Raithby and G. E. Schneider, Numerical solution of problems in incompressible fluid flow: treatment of the velocity–pressure coupling, *Numer. Heat Transfer* **2,** 417–440 (1979).
29. K. Velusamy, Introduction of whole field solution procedure and porous body formulations in THYC-2D, Internal Note: PFBR/66040/DN/1041/R-A, IGCAR (1989).